KSME

Springer

Journal of Mechanical Science and Technology 35 (11) 2021

Original Article
DOI 10.1007/s12206-021-1038-6

Keywords:
· Ecofriendly
· Refrigerants
· Anodization
· Porous coating
· R717 (Ammonia)
· Comparative study

Correspondence to:
A. Brusly Solomon
abruslysolomon@gmail.com

Citation:
Sudhan, A. L. S., Solomon, A. B., Immanuel, I. D. (2021). Comparative study on the heat transfer performance of micro-grooved anodized thermosyphon with R134a, R600a and R717 for low-temperature applications. Journal of Mechanical Science and Technology 35 (11) (2021) 5213~5223.
http://doi.org/10.1007/s12206-021-1038-6

Received March 29th, 2021
Revised July 6th, 2021
Accepted August 4th, 2021

† Recommended by Editor
Tong Seop Kim

Comparative study on the heat transfer performance of micro-grooved anodized thermosyphon with R134a, R600a and R717 for low-temperature applications

A. L. Sriram Sudhan, A. Brusly Solomon and I. Darwin Immanuel

Micro and Nano Heat Transfer Lab, Centre for Research in Material Science and Thermal Management, Department of Mechanical Engineering, Karunya Institute of Technology and Sciences, Coimbatore, India

Abstract A comparative heat transfer performance of an internally grooved anodized thermosyphon with eco-friendly refrigerants is presented in this study. Thermosiphons are fabricated with 50 numbers of axial micro-grooves having a width of 500 μm and a depth of 550 μm that is formed using an electrical discharge machining process. The micro-grooved surface was then anodized and characterized using SEM as well as DSA 25 drop shape analyzer. Later, the heat transfer performance of non-anodized grooved thermosyphon is studied by varying fill ratio (20-80 %), inclination angle (0-90°), and heat inputs (5-50 W). The heat transfer coefficient of the thermosyphon is improved by anodization by 20.9 %, 17.2 %, and 18.1 %, respectively, with R717, R134a, and R600a at optimum circumstances (30 % fill ratio and 60° inclination angle). Due to the performance enhancement and zero global warming potential of R717, an anodized surface with the same is recommended for a wide range of heat transfer applications.

1. Introduction

Due to the continuous addition of advanced features and miniaturization of electronic products, the heat generated from the processor device is escalating. Hence, conventional cooling methods and adding extended surfaces with natural and forced convection mechanisms are insufficient to meet the modern-day cooling demand. Therefore, necessary modifications were made to the traditional cooling systems. Introducing mini channels, microchannels, mini channel heat exchangers, and extended surfaces are some of the advancements made in the electronic cooling systems [1-5] to sustain the cooling demand. However, two-phase passive heat transfer devices such as heat pipes and thermosyphons are attracted to various electronic cooling applications due to their passive nature. A phase change wickless heat transfer device called thermosyphon works with the aid of gravity. The circulation of the fluid from the condenser to the evaporator takes place without an external pumping source. A phase change working fluid is used in a heat transfer device to transmit heat from one side to the other, employing its motion [6, 7]. It was noticed that the conventional working fluid in the thermosyphon is replaced with nanofluid to enhance the thermal performance of thermosyphons [8-16]. Moreover, the traditional fluids and nanosuspensions are utilized in thermosyphons to use in high-temperature applications. Later, refrigerants such as R134a, R600a, Freon, R404a and anhydrous Ammonia were applied in thermosyphons for lower heat transfer applications [17-19]. Later, refrigerant charged heat pipes and thermosyphons were used in solar cookers and water heaters [20, 21] for the heat exchange process and found efficient over conventional fluid charged heat pipes. Apart from using working fluids, surface enhancement also plays an essential role in the heat transfer enhancement of thermosyphons. Surface enhancement techniques include the addition of fins, internal surface coating, construction of micro-grooves in the inner surface of the thermosiphon [22, 23]. One of the coating methods used in our previous

research is the anodization technique which converts the aluminium in to aluminium oxide (AAO). In previous research, the anodized surface was formed in heat pipes, thermosyphons, and flat thermosyphons of various shapes (cylindrical, grooved heat pipes, plain and grooved thermosyphons, and flat thermosyphons) and their performance was investigated using various working fluids (acetone, R134a, and R600a) for higher heat loads [34-41]. It is understood that the alterations made in the inner surface of thermosyphon through anodization process develop more active nucleation sites, and lead to performance enhancement in the evaporator heat transfer due to enhancement in the boiling process. Though the conventional fluids were used in anodized thermosyphons for high-temperature applications, liquid ammonia in anodized micro finned thermosiphon is new, and it is essential for compact electronics operating at low temperatures. Therefore, this study focuses on studying the heat transfer characteristics using R134a, R600a and R717 as working fluids due to their lower boiling point than other refrigerants. Moreover, it is necessary to compare all the fluids in the same geometry, especially with an anodized surface to identify the best combination of surface and fluid for the electronic cooling applications. Hence, this research work is aimed to form a uniform and ordered pores with more active nucleation sites in the grooved thermosyphon's internal surface and study how anodization's effect plays a significant role in heat transfer in the evaporator and condenser section. Additionally, this work also studies the comparative heat transfer performance with R134a, R600a, and R717 as working fluids with the optimum fill ratio and optimum inclination angle identified at lower heat loads. This study may help the research fraternity to find the best combination surface and working fluid, which has not been reported in any other literature exclusively for low-temperature applications.

2. Experimental procedure

2.1 Manufacturing of anodized aluminium grooved thermosyphon

Grooved thermosyphon is fabricated using an aluminium tube with an OD of 19 mm, ID of 16.8 mm, and a length of 350 mm. Initially, the rectangular microgrooves of 50 numbers with a width of 500 μm and a depth of 550 μm are formed using a wire cutting EDM method. The anodization technique was then carried out to make a thin porous coating at the thermosyphon's inner surface. The detailed anodization procedure used in the presented study is reported in our previous studies [39]. The surface morphology, pore size as well as the contact angle are measured for the anodized surface. The contact angle of anodized aluminium grooved thermosyphon is measured using DSA25 (drop shape analyzer) with a range of 0° to 180°, which was observed to be < 10°. Then both the ends of the aluminium grooved thermosyphon are closed with the end caps. One end cap carries the charging tube. After cleaning and necessary evacuation process, working fluid is charged into the grooved thermosyphon. Finally, the heating coil made with nichrome wire of two layers is winded on the evaporator surface to provide the heat.

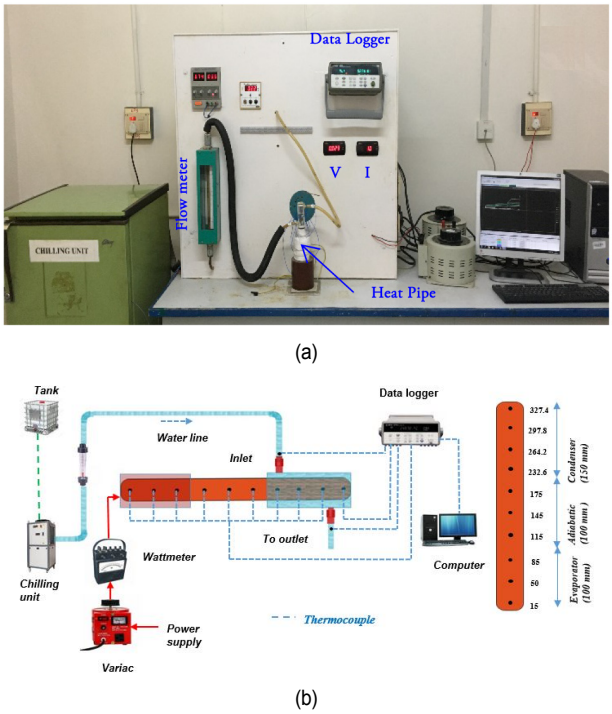

Fig. 1. View of experimental set up: (a) photographic; (b) schematic.

2.2 Experimental analysis

The illustrative representation of the experimental set-up and schematic view of the experimental set-up used in the study is presented in Figs. 1(a) and (b). The experimental set-up (Fig. 1(a)) consists of five basic units, classified as the chilling unit with the range of 0-50 °C, power source unit, a wattmeter with the range of 0-500 W, flow meter operating between 0-50 LPH, and data logger unit (20 channel). The complete experimental structure and experimental details are available in our previous studies [35]. After all set, heat input was applied in the evaporator using dimmer stat and the heat supply was monitored using voltmeter and ammeter connected across the heating coil. There are twelve thermocouples with ±0.2 % accuracy in which 3 numbers in the evaporator, 3 in adiabatic and 4 in the condenser are used as shown in Fig. 1(b). One thermocouple each in the inlet and outlet of the condenser cooling jacket was also fixed. All thermocouples attached to the experimental set-up are connected with a data logger unit where the temperatures are recorded and displayed.

Once the heat input is supplied, the thermocouples attached at different thermosyphon positions show the temperature for every 30 seconds. After the steady-state achieved, the succeeding heat input shall be given with an interval of 5 watts. In this study, evaporator temperatures T_e is the average of T_1, T_2 and T_3. The adiabatic temperature T_a is the average of T_4, T_5,

and T_6. The condenser temperature T_c is the average of T_7, T_8, T_9, and T_{10}. The inlet and outlet water temperatures are taken from T_{11} and T_{12}. The condenser section of the thermosyphon was cooled by the continuous circulation of cooling water from the chiller with a constant mass flow rate of 20 LPH at a temperature of 10 °C.

The performance of thermosyphons is evaluated using the heat balance test. The heat provided in the evaporator section is estimated using Eq. (1).

$$Q_{in} = V \times I \tag{1}$$

where V and I are the voltage and current supplied. The heat transported by the thermosyphon is estimated using the Newton law of cooling, as shown in Eq. (2).

$$Q_{out} = m_l \times C_{p,l} \times \left(T_{out} - T_{in}\right) \tag{2}$$

where $m_l, C_{p,l}, T_{in}, T_{out}, Q_{in}$ and Q_{out} are mass flow rate at the condenser section, the specific heat capacity of water, inlet water temperature, outlet water temperature, heat source, and heat released.

The total resistance of the thermosiphon is calculated as

$$R_t = \frac{T_{ew} - T_{cw}}{Q_{output}} \tag{3}$$

and the thermal resistance at the evaporator and condenser is calculated using Eqs. (4) and (5), respectively

$$R_e = \frac{T_{ew} - T_a}{Q_{input}} \tag{4}$$

$$R_c = \frac{T_a - T_{cw}}{Q_{output}} \tag{5}$$

In this study, the adiabatic temperature T_a is taken as a vapour temperature throughout the experiment. Temperatures T_e, T_a and T_c are the average temperatures of evaporator, adiabatic and condenser.

The heat transfer coefficients at the evaporation and condenser section are estimated by using the Eqs. (6) and (7)

$$h_e = \frac{Q_{input}}{A_e \times (T_{ew} - T_a)} \tag{6}$$

$$h_c = \frac{Q_{Output}}{A_c \times \left(T_a - T_{cw}\right)} \tag{7}$$

A_e, A_c, h_e and h_c are the evaporator area, condenser area, evaporator and condenser heat transfer coefficient. To check whether the anodization affects the maximum heat transfer limits, boiling limit, sonic limit and flooding limit of the thermosiphon is calculated using Eqs. (8)-(10) [42]

$$Q_{boil} = 0.12 \times \left(2\pi \times R_h\right) \times h_{fg} \rho_v^{0.5} \times \left\{\sigma g \left(\rho_l - \rho_v\right)\right\}^{0.25} \tag{8}$$

and, the sonic limit of the thermosiphon is calculated as

$$Q_{sonic} = \rho_v \times h_{fg} \times A_v \left(\frac{\gamma R_v T_v}{2\left[\gamma + 1\right]}\right) \tag{9}$$

The flooding limit concerning adiabatic vapour temperature calculated as below

$$Q_{flooding} = K h_{fg} A_t \left[\sigma g \left(\rho_l - \rho_v\right)\right]^{0.25} \times \left(\rho_l^{-0.25} + \rho_v^{-0.25}\right)^{-2} \tag{10}$$

The thermophysical properties of R134a and R717 are taken from ASHRAE Handbook [43, 44], and same for R600a was taken from ASHRAE, 2009, vapour density was taken from R.D. Goodwin, 1982 for different vapour temperatures as shown in Table 1.

Total global warming potential is calculated using Eq. (11) [46]. GWP indicates the global warming potential, L represents the leakage rate of the refrigerant per year, n, m and α are the system operating time, amount of refrigerant filled in thermosyphon and recycling factor of the refrigerant

$$\begin{aligned}&\text{Direct global warming potential}\\&= \left\{GWP \times L \times n\right\} + \left\{GWP \times m \times \left(1 - \alpha\right)\right\}\end{aligned} \tag{11}$$

The uncertainties in the heat load, heat transfer coefficient (average of both evaporator and condenser), and thermal resistances are 1.42 %, 4.85 %, 5.51 %, and 4.45 %.

3. Results and discussions

After the anodization process was completed, a sample piece of anodized aluminium grooved pipe is analyzed using SEM. Its surface morphology and contact angle are presented in Figs. 2(a)-(c). From the SEM image, it was understood that a thin oxide layer (porous structure) formed at the inner surface of the grooved thermosyphon with a pore size of 2.053 μm due to the anodization.

The contact angle of non-anodized surface using DI water as measuring liquid is about 110 degree as presented in Fig. 2(c), but the same for anodized surface is found to be less than 10 degree, which is very difficult to measure due to their high wetting characteristics of the surface. After the characterization of the surface, the performance of thermosyphon was studied. The heat transfer performance of non-anodized grooved thermosyphon was analyzed using R134a, R600a and R717 as a working fluid while varying fill ratio between 20-80 %, inclination angle between 0-90° with lower heat input (5-50 W).

Table 1. Thermophysical properties of refrigerants.

Refrigerant (R134a)	Non-anodized				Anodized			
Heat input (W)	Vapour temperature (°C)	Liquid density (Kg/m^3)	Vapour density (Kg/m^3)	Surface tension (N/m)	Vapour temperature (°C)	Liquid density (Kg/m^3)	Vapour density (Kg/m^3)	Surface tension (N/m)
5	18.15	1232.16	26.18	0.009	17.42	1234.71	25.59	0.0091
10	18.83	1228.95	26.78	0.0089	18.45	1232.16	26.81	0.0089
15	20.87	1221.65	28.50	0.0086	19.65	1226.75	27.46	0.0088
20	22.21	1218.20	29.43	0.0084	20.56	1221.65	29.46	0.0086
25	23.46	1212.55	30.81	0.0083	21.77	1218.83	29.29	0.0085
30	25.53	1204.79	32.82	0.0080	22.73	1214.25	30.14	0.0083
35	26.08	1202.9	33.34	0.0079	23.62	1212.55	30.85	0.0082
40	28.016	1195.2	35.34	0.0076	24.59	1208.25	31.88	0.0081
45	29.814	1188.26	37.30	0.0075	25.52	1204.79	32.82	0.0080
50	30.90	1183.55	38.50	0.0073	27.49	1197.15	34.78	0.0077
Refrigerant (R600a)	Non-anodized				Anodized			
Heat input (W)	Vapour temperature (°C)	Liquid density (Kg/m^3)	Vapour density (Kg/m^3)	Surface tension (N/m)	Vapour temperature (°C)	Liquid density (Kg/m^3)	Vapour density (Kg/m^3)	Surface tension (N/m)
5	18.37	559.3	7.51	0.01086	17.307	560.15	5.41	0.01086
10	19.89	557.13	7.95	0.01069	19.93	557.13	7.95	0.01069
15	20.57	556.2	8.03	0.01061	20.54	556.2	8.03	0.01061
20	21.35	555.65	8.21	0.01054	21.21	555.4	8.21	0.01054
25	23.17	553.15	8.64	0.010309	22.4	553.89	8.45	0.010403
30	25.01	550.65	9.09	0.001007	23.22	553.15	8.64	0.010309
35	26.21	549.4	9.40	0.0099	24.21	551.9	8.89	0.01019
40	27.18	548.15	9.67	0.00996	25.23	550.6	9.09	0.01007
45	28.84	545.7	10.12	0.00985	25.90	549.52	9.32	0.00999
50	29.48	545.07	10.35	0.00959	26.75	548.46	9.54	0.0099
Refrigerant (R717)	Non-anodized				Anodized			
Heat input (W)	Vapour temperature (°C)	Liquid density (Kg/m^3)	Vapour density (Kg/m^3)	Surface tension (N/m)	Vapour temperature (°C)	Liquid density (Kg/m^3)	Vapour density (Kg/m^3)	Surface tension (N/m)
5	17.16	614.3	6.07	0.0224	15.82	616.2	5.84	0.0226
10	18.82	611.9	6.42	0.02205	17.00	614.5	6.07	0.0224
15	20.20	610.2	6.69	0.00217	18.59	612.2	6.37	0.0220
20	21.53	607.9	6.97	0.0213	19.13	611.6	6.48	0.0219
25	23.02	605.7	7.30	0.02092	20.28	610.2	6.68	0.0217
30	24.05	602.8	7.53	0.0208	21.08	608.7	6.87	0.0214
35	25.59	601.9	7.89	0.0205	21.85	607.4	7.04	0.0213
40	27.02	599.7	8.247	0.0202	22.46	606.5	7.17	0.0209
45	28.60	597.3	8.64	0.0197	23.67	604.7	7.45	0.0211
50	30.3	595.2	9.07	0.0195	24.91	602.9	7.73	0.0205

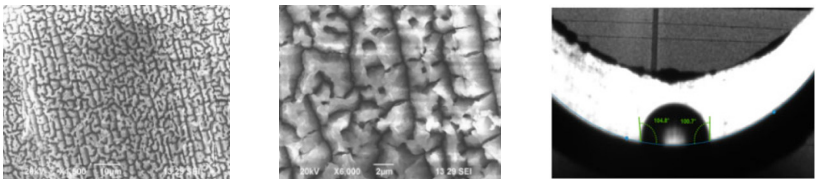

(a) (b) (c)

Fig. 2. SEM image of anodized grooved aluminium pipe at 20 °C: (a) magnification at 1500; (b) magnification at 6000; (c) contact angel of non-anodized surface.

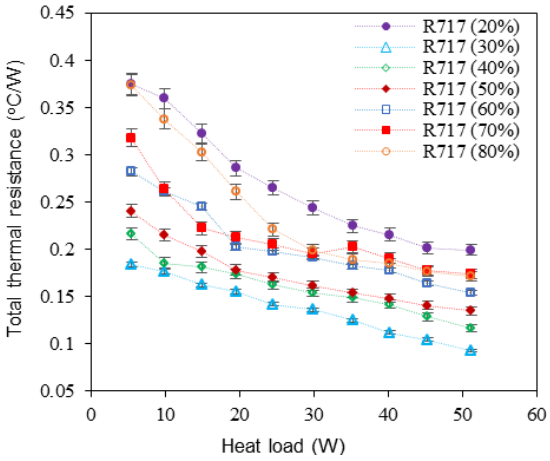

Fig. 3. Variation in the thermal resistance of non-anodized grooved thermosyphon at different heat loads and fill ratios.

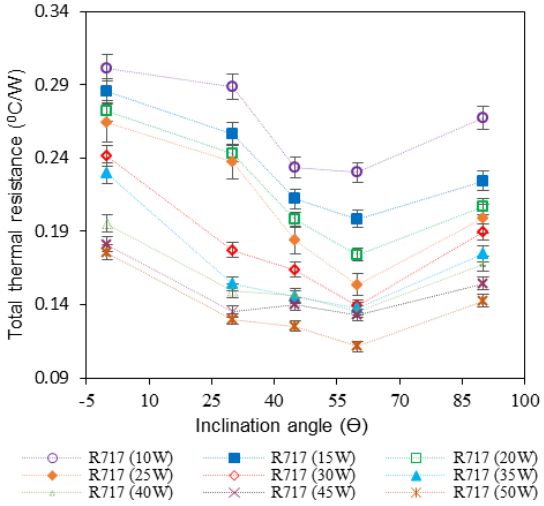

Fig. 4. Total thermal resistance variation with inclination angle of non-anodized grooved thermosyphon using R717 as a working fluid.

3.1 Effect of fill ratio on the total thermal resistance of non-anodized grooved thermosyphon

The significance of the fill ratio (20 %-80 %) on the total thermal resistance of non-anodized grooved thermosyphon using R717 concerning heat load was calculated using Eqs. (3)-(5) and illustrated in Fig. 3. The analysis showed a decreasing trend of thermal resistance with the increase in heat load for all the fill ratios. Also noticed that the thermal resistance of the thermosyphon charged with 20 % fill ratio is higher than the same with other fill ratios for all heat inputs. This higher resistance may be due to the starvation of working fluid in the evaporator. Increasing the fill ratio from 20 % to 30 % resulted in a sudden drop in thermal resistance. This sudden change in thermal resistance may be due to the adequate circulation of working fluids from the condenser to the evaporator. Further, an increase in fill ratio from 30 % to a higher fill ratio resulted in a linear increase in thermal resistance. The other fill ratio or excess quantity of fluid in the evaporator lead to additional resistance and thus increases the total resistance of the thermosyphon. Moreover, the highest reduction in thermal resistance of 0.092 °C/W was observed in a 30 % fill ratio, which is considered an optimum fill ratio for maximum heat transfer. This reduction in thermal resistance is due to the thin liquid film formed at the evaporator section. Further increase in filling quantity lead to excess working fluid inventory in the evaporator leads to higher liquid film thickness and to higher resistance.

3.2 Effect of inclination angle on the total thermal resistance of thermosyphon using R717

The significance of the inclination angle (0-90°) on the overall thermal resistance of non-anodized grooved thermosyphon was calculated using Eq. (3) while testing R717 with the optimum fill ratio of 30 % and presented in Fig. 4. It was found that the thermal resistance followed a decreasing trend up to 60° when the inclination angle was increased for all three working fluids at all heat loads. The inclination angle of 60° is found to be optimum for maximum heat transfer for both cases. This optimum inclination may be due to the adequate circulation of working fluid from condenser to evaporator at the optimum fill ratio of 30 %. As the inclination angle increases, the gravity effect increases, resulting in adequate fluid circulation and decreasing resistance. At the inclination of 60°, the liquid circulation may be maximum, resulting in the lowest resistance. At 90° inclination, the resistance is increasing due to forming a liquid pool as the gravity attracts condensed liquid. Similarly, a decreasing trend in thermal resistance and the optimum inclination angle of 60° were observed for R134a and R600a as a working fluid. The above optimum conditions are used to test anodized grooved thermosyphon with R134a, R600a, and R717 as working fluids.

3.3 The effect of anodization on the total thermal resistance of grooved thermosyphon

The variation in total thermal resistance for both non-anodized and anodized grooved thermosyphon with R134a, R600a, and R717 as working fluids was calculated using Eq. (3) and presented in Fig. 5(a). For R134a, R600a, and R717, an exponential decrease in thermal resistance was observed with increased heat input for both non-anodized and anodized cases. The anodization of thermosyphon's inner wall surface promotes the generation of active nucleation sites and surface wettability. This higher wettable surface enhances the rewetting of hotspots, resulting in a further reduction in thermal resistance and the surface temperature difference [35, 36]. Moreover, comparing three refrigerants, anodized thermosyphon's thermal resistance with R717 shows a maximum reduction of 34.4 % compared to the non-anodized case. Anodized thermo-

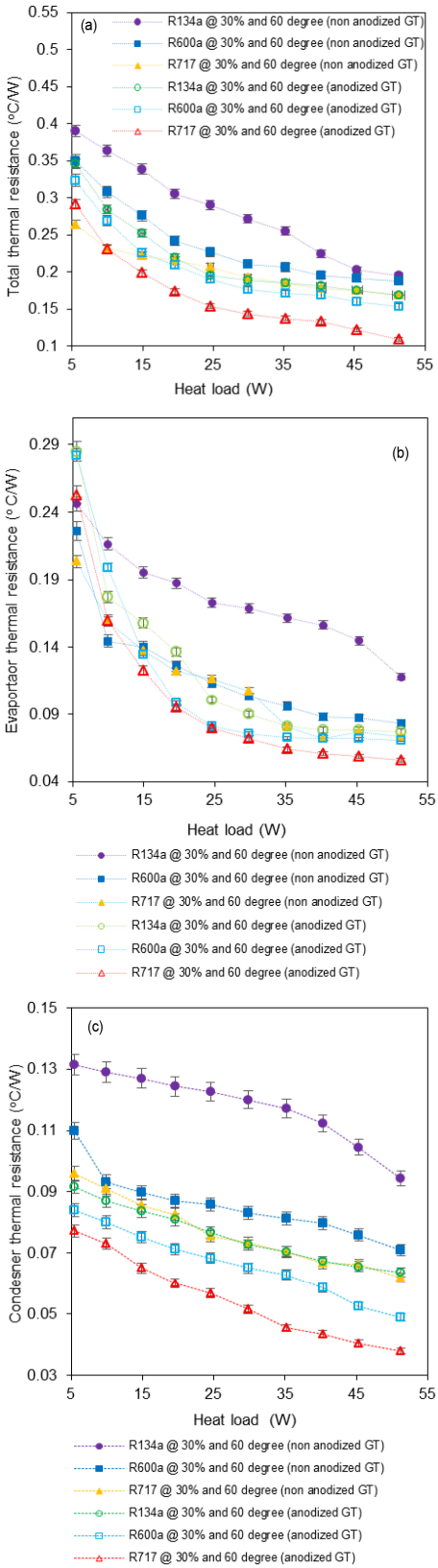

Fig. 5. (a) Total thermal resistance; (b) evaporator thermal resistance; (c) condenser thermal resistance of non-anodized and anodized grooved thermosyphon at optimum conditions using R134a, R600a and R717 as a working fluid.

syphon's thermal resistance with R134a and R600a reduced 14.22 % and 17.77 % respectively compared to the non-anodized case. The difference in evaporator thermal resistance for both non-anodized and anodized cases using R134a, R600a, and R717 as working fluid at an optimum fill ratio of 30 % and an inclination angle of 60° was calculated using Eq. (4) and illustrated in Fig. 5(b). In this analysis, the exponentially decreasing curve was observed for evaporator thermal resistance with an increase in heat loads for both non-anodized and anodized grooved cases at optimum fill ratio and inclination angle. Moreover, the lowest thermal resistance profile was found in the anodized grooved thermosyphon with R717 than R134a and R600a. The variation in condenser thermal resistance with increasing heat input for all the working fluids was calculated using Eq. (5) and illustrated in Fig. 5(c). The exponentially decreasing trend with increasing heat input was observed as same as in Figs. 5(a) and (b). Further, the difference between vapour (adiabatic) temperature and condenser wall temperature increases dependently with heat loads and at a higher heat load of 50W shows more temperature difference. On comparing all three refrigerants, R717 shows the highest reduction in condenser thermal resistance of about 40.6 % than the non-anodized case. This reduction in thermal resistance is occurred, possibly due to the surface tension of the working fluid. R717 has higher surface tension than R134a and R600a, results in more transportation of the condensed liquid to the evaporator in R717 charged grooved thermosyphon, which leads to a reduction in the condenser thermal resistance.

3.4 The effect of anodization on the evaporator and condenser heat transfer coefficient of grooved thermosyphon

Fig. 6(a) presents the evaporator's heat transfer coefficient of both non-anodized and anodized grooved thermosyphons using R134a, R600a, and R717 for different heat inputs. A linear increasing curve with an increase in heat input was obtained for the heat transfer coefficient and attained a maximum at a higher heat input of 50 W. Moreover, the anodized thermosyphon's heat transfer coefficient seems higher than the non-anodized case for all the refrigerants. Further, an enhancement of 20.9 % was observed for R717 with anodization over non-anodized thermosyphon. Similarly, the anodized thermosyphon with R134a and R600a showed an enhancement of 17.2 % and 18.1 %, respectively, compared to the non-anodized grooved thermosyphon. The enhancement in the evaporator heat transfer coefficient is due to the anodization process. The anodization process forms a thin porous coating that enhances the evaporation and boiling heat transfer. Further, the anodization process enhances the porosity, the generation of additional active nucleation sites which promotes the nucleate boiling, liquid absorbing capability and the increase in surface area results in an enhancement in evaporation heat transfer [47]. The variation in the condenser heat transfer coefficient of non-anodized and anodized grooved thermosyphon

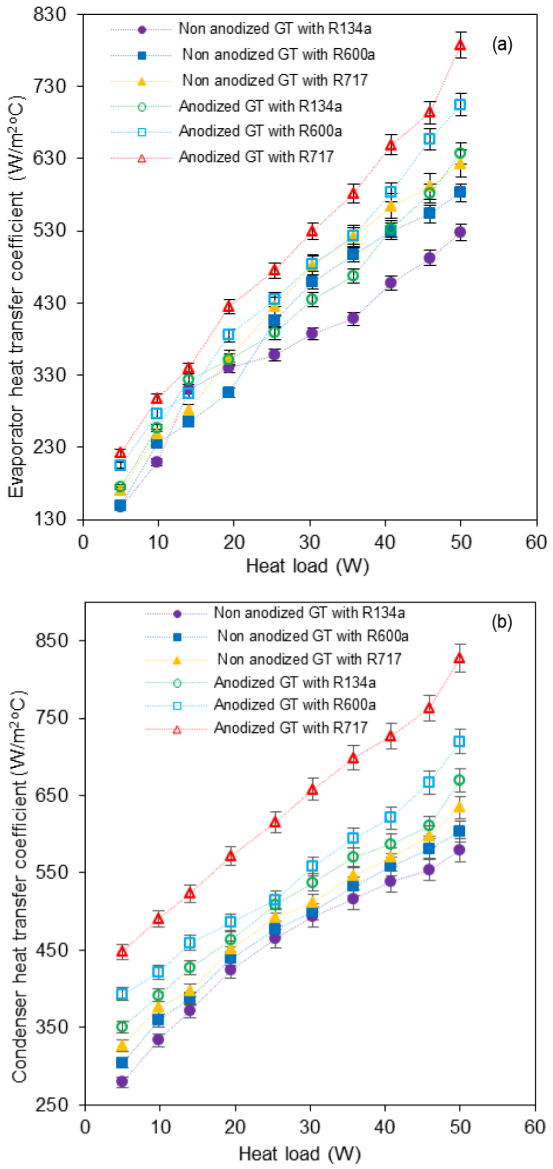

Fig. 6. Variations in (a) evaporator heat transfer coefficient; (b) condenser heat transfer coefficient of non-anodized and anodized grooved thermosyphon at optimum conditions using R134a. R600a and R717 at different heat loads.

with an increase in heat input was calculated using Eq. (7) and illustrated in Fig. 6(b). An exponential increase in condenser heat transfer with an increase in heat input was noticed. It was also noticed that the anodized grooved thermosyphon with R717 showed more enhancement at the condenser side due to thin-film condensation on comparing with R134a and R600a. Moreover, it was observed that the heat transfer coefficient in the condenser is more significant than in the evaporator of thermosyphon. This variation may be due to the heat transfer mechanisms involved in the respective thermosyphon sections evaporator and condenser respectively. Nucleate boiling in the evaporator and film condensation in the condenser is expected. In general, the heat transfer coefficient due to the condensation is higher than the same due to the boiling process. The anodization process enhances the boiling resulting higher mass of vapor flow from evaporator to condenser and same is condensed in the condenser results in higher heat transfer coefficient. A similar trend was observed in our previous study [35] also. Further, the superior thermo-physical properties of Ammonia with the combination of anodized surface further increase the performance of thermosyphon over the application of R134a and R600a.

3.5 Effect of anodization on the heat transport limitations of grooved thermosyphon

The effect of anodization on the boiling limit of grooved thermosyphon with R134a, R600a, and R717 was calculated using Eq. (8) [42] and presented in Fig. 7(a). It was found that the boiling limit increases slightly with an increase in adiabatic vapour temperature for both non-anodized and anodized grooved thermosyphon for all three working fluids. Further, it was found that the non-anodized and anodized grooved thermosyphon using R717 showed a highest boiling limit than with the same of R134a and R600a. This higher boiling limit was due to the high latent heat of vaporization and lower vapour density of R717. This increase in boiling limit suggests that the thermosyphon can be operated with additional radial heat flux. The sonic limit of thermosyphons for different adiabatic vapour temperature was calculated using Eq. (9) and presented in Fig. 7(b). It was found that the R717 showed a higher sonic limit compared to R134a and R600a for both non-anodized and anodized grooved thermosyphon. The flooding limit of grooved thermosyphon using R134a, R600a, and R717 as working fluids was calculated using Eq. (10) and presented in Fig. 7(c). It was found that the flooding limit of thermosyphons with all refrigerants increases with adiabatic vapour temperature. However, the flooding limit of R717 is higher than the same of R134a and R600a due to higher vapour velocities. This increase in heat transfer limitations indicates that the combination anodized thermosyphon with R717 has higher operational capability than the other working fluid and surface combination.

3.6 Discussions on total equivalent warming impact

Quantitative analysis on the emission, effect of environmental and economic aspects of using alternative fuels in automobile engines was studied [48-51]. It was clearly stated that the use of alternative fuels in automobile engines reduces the global warming potential and greenhouse gases in the surroundings, which lead to a healthy atmosphere. Similarly, to analyze the effect of using refrigerants on the global warming potential, the total equivalent warming impact (TEWI) for three working fluids (R134a, R600a and R717) was calculated using Eq. (11). TEWI study measures the total global warming influence on the atmosphere due to the direct and indirect global warming potential. Direct global warming may have resulted

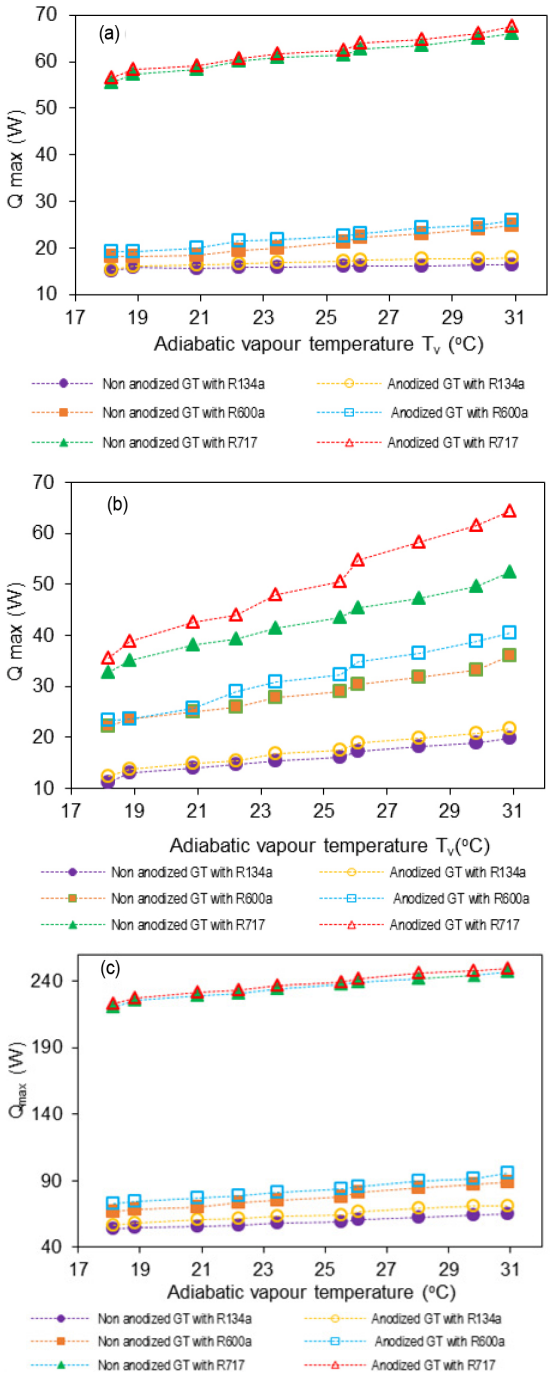

Fig. 7. Variations in (a) boiling limit; (b) sonic limit; (c) flooding limit at different vapour temperature for R134a, R 600a and R717.

from the ground sources such as refrigerant leakage and indirect global warming due to the burning of fossil fuels. Since the system operates at the ground level, this study concentrates only on direct global warming potential by neglecting the indirect global warming potential. The amount of refrigerant filled in the thermosyphons under optimum condition is 0.02721 kg, 0.01291 kg and 0.01359 kg, respectively, for R134a, R600a and R717. The leakage rate of thermosyphon considered per

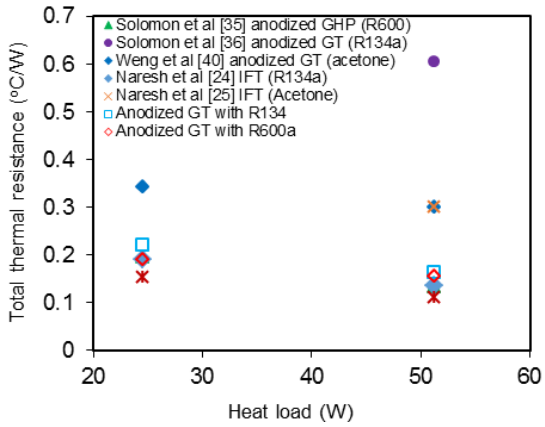

Fig. 8. Comparison of overall thermal resistances of anodized GT working with R134a, R600a, acetone and R717.

year was 0.0136, 0.0064 and 0.00679, respectively for R134a, R600a and R717. The total equivalent warming impact was calculated for 10 years, with 0.7 recycling factor. The analysis found that the direct global warming potential of R134a, R600a and R717 are 206.15, 0.336 and 0. It was also found that the global warming potential with the application of R717 was zero. Hence, this study recommends using R717 with an anodized surface for a wide range of applications due to zero global warming potential.

3.7 Validation of total thermal resistance of anodized thermosyphon with similar studies

Fig. 8 presents the comparisons of the overall thermal resistance of internally finned thermosyphon and anodized GT from the published works. The comparison shows that the thermal resistance profile of internally finned and anodized GT is lower than the resistance reported in the previous studies. The above results indicate that the combination of anodized GT with ammonia outperforms previous studies.

4. Conclusion

The thermal performance of non-anodized and anodized grooved thermosyphon has been investigated experimentally. The effect of anodization on the thermal resistance, heat transfer coefficient, wall temperatures, and heat transport limitations was studied at an optimum fill ratio and inclination angle. The following conclusions were drawn from the above-obtained results.

- The optimum fill ratio was found to be 30 % and the inclination angle was 60° while using R134a, R600a, and R717 as working fluids.
- The anodized grooved thermosyphon with the R717 showed maximum thermal resistance reduction of 34.4 % than R134a and R600a with 14.22 % and 17.77 %, respectively. Similarly, a maximum heat transfer coefficient

enhancement of 20.9 % was observed for R717 with anodization than R134a and R600a of 17.2 % and 18.1%, respectively.

- The anodized grooved thermosyphon with R717 extends the heat transport limitations concerning boiling, sonic and flooding limitations than R134a and R600a.
- As the thermosyphon anodized surface and R717 showed the highest performance, this combination may be suitable for lightweight low-temperature electronic cooling applications.

Acknowledgement

The authors are grateful to the DST-SERB (DST/SERB/YSS/2015/001084) for financially supporting this research work. The authors also express their gratitude to Mr. Jayaseelan, Karunya Institute of Technology and Sciences, for assisting fabrication and testing.

Nomenclature

D	: Depth of the groove (m)
W	: Width of the groove (m)
σ	: Surface tension (N/m)
e	: Coating thickness (m)
V_{in}	: Voltage (v)
I_{in}	: Current (A)
Q_{in}	: Heat input (Watts)
L_{eff}	: Effective length of thermosyphon (mm)
μ_l	: Liquid viscosity (Ns/m^2)
μ_v	: Vapour viscosity (Ns/m^2)
ρ_l	: Liquid density (Kg/m^3)
ρ_v	: Vapour density (Kg/m^3)
A	: Heat transfer area (m^2)
λ	: Latent heat of vaporization (J/kg)
m_{rate}	: Mass flow rate (kg/s)
$C_{p\,l}$	: Specific heat capacity of liquid (J/kgK)
T	: Temperature (°C)
Q_{out}	: Heat rejected from the condenser (kg/s)
G	: Acceleration due to gravity (m/s^2)
L_t	: Total length (mm)
R_{th}	: Thermal resistance (°C/W)
h	: Heat transfer coefficient (W/m^2. °C)
GT	: Grooved thermosyphon
LPH	: Liters per hour

Greek symbol

θ	: Inclination angle

Subscripts

in	: Inlet
out	: Outlet
eff	: Effective
t	: Thermosyphon
p	: Pressure
v	: Vapour
l	: Liquid
c, w	: Condenser wall
e, w	: Evaporator wall

References

[1] M. Mohammadifar, E. Rasouli and M. R. Hajmohammadi, Optimal design and placement of heat sink elements attached on a cylindrical heat-generating body for maximum cooling performance, *Thermochim. Acta.* (2021) 3-5.

[2] S. M. Ayatollahi, A. Ahmadpour and M. R. Hajmohammadi, Performance evaluation and optimization of flattened microchannel heat sinks for the electronic cooling application, *J. Therm. Anal. Calorim.,* March (2021) 1-16.

[3] M. R. Hajmohammadi and M. Mohammadifar, Optimal placement and sizing of heat sink attachments on a heat-generating piece for minimization of peak temperature, *Thermochim. Acta.*, 689 (2020) 178645.

[4] M. R. Hajmohammadi, E. Rasouli and M. A. Elmi, Geometric optimization of a highly conductive insert intruding an annular fin, *Int. J. Heat Mass Transf.*, 146 (2020) 118910.

[5] T. Wu et al., Multitasking multi-objective operation optimization of integrated energy system considering biogas-solar-wind renewables, *Energy Convers. Manag.,* 229 (2021) 3-5.

[6] G. Murali, K. Mayilsamy and T. V Arjunan, An experimental study of PCM incorporated thermosyphon solar water heating system, *Int. J. Green Energy,* 12 (9) (2015) 1-43.

[7] H. Jouhara and A. J. Robinson, Experimental investigation of small diameter two-phase closed thermosyphons charged with water, FC-84, FC-77 and FC-3283, *Appl. Therm. Eng.*, 30 (2-3) (2010) 201-211.

[8] V. Kiseev and O. Sazhin, Heat transfer enhancement in a loop thermosyphon using nanoparticles/water nanofluid, *Int. J. Heat Mass Transf.*, 132 (2019) 557-564.

[9] A. Ozsoy and V. Corumlu, Thermal performance of a thermosyphon heat pipe evacuated tube solar collector using silver-water nanofluid for commercial applications, *Renew. Energy.*, 122 (2018) 26-34.

[10] T. Grab et al., Operation performance of thermosyphons employing titania and gold nanofluids, *Int. J. Therm. Sci.*, 86 (2014) 352-364.

[11] M. Ramezanizadeh, M. A. Nazari and M. Hossein, Experimental and numerical analysis of a nanofluidic thermosyphon heat exchanger, *Eng. Appl. Comput. Fluid Mech.*, 13 (1) (2019) 40-47.

[12] H. Ghorabaee et al., Effect of nanofluid and surfactant on thermosyphon heat pipe performance, *Heat Transf. Eng.*, 41 (20) (2019) 1829-1842.

[13] A. Kujawska et al., Impact of silica nanofluid deposition on thermosyphon performance, *Heat Transf. Eng.* (2020).

[14] S. Torii, Y. Satou and Y. Koito, Experimental study on convective thermal-fluid flow transport phenomena in circular

tube using nanofluids, *Int. J. Green Energy*., 7 (3) (2010) 289-299.

[15] S. H. Oh et al., Experimental study on heat transfer performance of a two-phase single thermosyphon using HFE-7100, *J. Mech. Sci. Technol.*, 31 (10) (2017) 4957-4964.

[16] S. Wannapakhe et al., Heat transfer rate of a closed-loop oscillating heat pipe with check valves using silver nanofluid as working fluid, *J. Mech. Sci. Technol.*, 23 (6) (2009) 1576-1582.

[17] A. Ozsoy and R. Yildirim, The performance of ground source heat pipes at low constant source temperatures, *Int. J. Green Energy*, 15 (11) (2018) 641-650.

[18] A. R. Anand, Investigations on effect of evaporator length on heat transport of axially grooved ammonia heat pipe, *Appl. Therm. Eng.*, 150 (2019) 1233-1242.

[19] A. L. Sriram et al., Application of environment-friendly refrigerants in anodized grooved thermosyphon at high heat loads, *Mater. Today Proc.,* 46 (2021) 138-140.

[20] M. Esen, Thermal performance of a solar cooker integrated vacuum-tube collector with heat pipes containing different refrigerants, *Solar Energy*, 76 (2004) 751-757.

[21] M. Esen and H. Esen, Experimental investigation of a two-phase closed thermosyphon solar water heater, 79 (5) (2005) 459-468.

[22] R. Nair and C. Balaji, Synergistic analysis of heat transfer characteristics of an internally finned two phase closed thermosyphon, *Appl. Therm. Eng.*, 101 (2016) 720-729.

[23] S. F. Li et al., Effect of nano-structure coating on thermal performance of thermosyphon boiling in micro-channels, *Int. J. Heat Mass Transf.*, 124 (2018) 463-474.

[24] Y. Naresh and C. Balaji, Thermal performance of an internally finned two phase closed thermosyphon with refrigerant R134a: A combined experimental and numerical study, *Int. J. Therm. Sci.*, 126 (2018) 281-293.

[25] Y. Naresh and C. Balaji, Experimental investigations of heat transfer from an internally finned two phase closed thermosyphon, *Appl. Therm. Eng.*, 112 (2017) 1658-1666.

[26] T. Sukchana and N. Pratinthong, Effect of bending position on heat transfer performance of R-134a two-phase close loop thermosyphon with an adiabatic section using flexible hoses, *Int. J. Heat Mass Transf.*, 114 (2017) 527-535.

[27] A. Bahmanabadi, M. Faegh and M. B. Shafii, Experimental examination of utilizing novel radially grooved surfaces in the evaporator of a thermosyphon heat pipe, *Appl. Therm. Eng.*, 169 (2020) 114975.

[28] Y. Kim et al., Effect of sintered microporous coating at the evaporator on the thermal performance of a two-phase closed thermosyphon, *Int. J. Heat Mass Transf.*, 131 (2019) 1064-1074.

[29] Y. Kim et al., Enhanced thermal performance of a thermosyphon for waste heat recovery: Microporous coating at evaporator and hydrophobic coating at condenser, *Appl. Therm. Eng.*, 175 (2020) 115332.

[30] P. Taylor et al., A study of the heat transfer characteristics of an FC-72 (C_6F_{14}) two-phase closed thermosyphon with helical grooves on the inner surface, *Heat Transf. Eng.*, 25 (8) (2004) 60-68.

[31] V. V Nirgude and S. K. Sahu, Nucleate boiling heat transfer performance of different laser processed copper surfaces, *Int. J. Green Energy*, 17 (1) (2019) 38-47.

[32] Y. D. Ling and S. Torii, Heat transfer enhancements in heat pipe constructed with a copper porous microstructure, *Int. J. Green Energy*, 18 (2) (2020) 166-171.

[33] W. Pinate, S. Rittidech and P. Meena, Critical heat flux of a two-phase closed thermosyphon with fins, *J. Mech. Sci. Technol.,* 32 (5) (2018) 2357-2364.

[34] A. B. Solomon et al., Performance enhancement of a two-phase closed thermosiphon with a thin porous copper coating, *Int. Commun. Heat Mass Transf.*, 82 (2017) 9-19.

[35] A. B. Solomon et al., Characterization of a grooved heat pipe with an anodized surface, *Heat Mass Transf. Und Stoffuebertragung*, 53 (3) (2017) 753-763.

[36] A. B. Solomon et al., Heat transfer performance of an anodized two-phase closed thermosyphon with refrigerant as working fluid, *Int. J. Heat Mass Transf.*, 82 (2015) 521-529.

[37] R. R. Singh et al., Effect of anodization on the heat transfer performance of flat thermosyphon, *Exp. Therm. Fluid Sci.*, 68 (2015) 574-581.

[38] R. R. Singh and A. B. Solomon, Effect of nucleation sites on the performance of anodized thermosyphon, *1st Int. ISHMT-ASTFE Heat Mass Transf. Conf.* (2015) 1-7.

[39] A. B. Solomon and M. Noel, Anodization and evaluation of an aluminium thermosyphon with anodized inner wall surface, *Energ* (2015) 1-9.

[40] H. C. Weng and M. H. Yang, Heat transfer performance enhancement of gravity heat pipes by growing aao nanotubes on inner wall surface, *Inventions*, 3 (42) (2018) 1-12.

[41] A. Varughese et al., Heat transfer characteristics and flow visualization of anodized flat thermosiphon, *Proc. Inst. Mech. Eng. Part E J. Process Mech. Eng.*, 234 (2) (2020) 182-192.

[42] S. H. Noie, M. R. S. Emami and M. Khoshnoodi, Effect of inclination angle and filling ratio on thermal performance of a two-phase closed thermosyphon under normal operating conditions, *Heat Transf. Eng.*, 28 (4) (2007) 365-371.

[43] ASHRAE, *Hand Book: Fundamentals, Chapter 30-Thermophysical Properties of Refrigerants*, EBSCO Publ. USA, 718 (2009) 1-39.

[44] A. Faghri, *Heat Pipe Science and Technology*, Taylor and Farncis, London (1995).

[45] W. M. H. R. D. Goodwin, *Thermophysical Properties of Isobutane from 114 to 700K at Pressures to 70 MPa*, NBS Publ. (1982) 1-200.

[46] T. Q. J. Fryer and K. Lee, *Methods of Calculating Total Equivalent Warming Impact (TEWI)*, Aust. Inst. Refrig. Air Cond. Heat. (2012) 21.

[47] L. L. Vasil'ev et al., Investigation of heat transfer by evaporation in capillary grooves with a porous coating, *J. Eng. Phys. Thermophys.*, 85 (2) (2012) 407-414.

[48] H. Gurbuz, The effect of H_2 purity on the combustion, performance, emissions, and energy costs, *Therm. Sci.*, 24 (1A) (2020) 37-49.

[49] H. Gürbüz, Evaluating effects of the Covid-19 pandemic period on energy consumption and enviro-economic indicators of Turkish road transportation, *Energy Sources, Part A: Recover. Util. Environ. Eff.* (2021) 1-4.
[50] H. Gürbüz, Ş. Yasin and H. Akçay, Environmental and enviroeconomic assessment of an LPG fueled SI engine at partial load, *J. Environ. Manage.,* 241 (2019) 631-636.
[51] Ş. Yasin and H. Gürbüz, A comparison of gasoline, liquid petroleum gas, and hydrogen utilization in an spark ignition engine in terms of environmental and economic indicators, *J. Energy Resour. Technol.*, 143 (5) (2021) 052301-052309.

Appendix

The following equations represent the uncertainty estimations for thermosyphon.

$$\frac{\Delta Q_{in}}{Q_{in}} = \sqrt{\left(\frac{\Delta V_{in}}{V_{in}}\right)^2 + \left(\frac{\Delta I_{in}}{I_{in}}\right)^2} \quad \text{(A.1)}$$

$$\frac{\Delta h}{h} = \sqrt{\left(\frac{\Delta q}{q}\right)^2 + \left(\frac{\Delta(\Delta T)}{\Delta T}\right)^2} \quad \text{(A.2)}$$

$$\frac{\Delta R}{R} = \sqrt{\left(\frac{\Delta Q_{in}}{Q_{in}}\right)^2 + \left(\frac{\Delta(\Delta T)}{\Delta T_{e,c}}\right)^2} \quad \text{(A.3)}$$

In the above equations ΔV_{in}, ΔI_{in}, V_{in} and I_{in} are the accuracy in voltage measurement, accuracy in measurement of current, input voltage, and input current. The q represents the heat flux given and the ΔT is the difference in temperature between the evaporative section and adiabatic section temperatures for h_e. And for h_c ΔT is the difference in temperature between the vapour and condenser wall.

Sriram Sudhan is currently working as a junior research fellow in the Mechanical Engineering Department at Karunya Institute of Technology and Sciences (KITS), Coimbatore. He is currently pursuing his Ph.D. in the area of electronic cooling. He has published 2 peer reviewed journal papers and 3 international conference papers.

Brusly Solomon is currently an Associate Professor in the Mechanical Engineering discipline at Karunya Institute of Technology and Sciences (KITS), Coimbatore. His research focuses on developing phase-change cooling devices such as heat pipes and thermosyphons for cooling applications. He has published over 40 artlcles in peer-reviewed international journals, 2 book chapters and over eight international conference proceedings. His research interests include phase change heat transfer, electronic cooling with heat pipes, natural convection heat transfer and Magnetic nanofluids.

Darwin Immanuel is currently a post graduate student in the Mechanical Engineering Department at Karunya Institute of Technology and Sciences (KITS), Coimbatore. His research interests focused on developing anodized grooved heat pipes for electronic cooling applications.